ACS Catalysis

Research Article

pubs.acs.org/acscatalysis

Roles of Ruthenium−Support Interactions of Size-Controlled Ruthenium Nanoparticles for the Product Distribution of Fischer−Tropsch Synthesis

Taeyoung Koh,[†] Hyun Mo Koo,[‡] Taekyung Yu,[§] Byungkwon Lim,*[,†] and Jong Wook Bae*[,‡]

[†]School of Advanced Materials Science and Engineering, [‡]School of Chemical Engineering, Sungkyunkwan University (SKKU), Suwon 440-746, Korea

[§]School of Chemical Engineering, Kyung Hee University, Yongin 446-701, Korea

Supporting Information

ABSTRACT: A simple aqueous-phase route to the synthesis of ruthenium (Ru) nanoparticles with size in the sub-2-nm regime was prepared by reducing $RuCl_3$ with $NaBH_4$ as a reducing agent in the presence of 6-aminohexanoic acid (AHA) as a capping agent. We found that AHA plays a key role in the formation and distribution of ultrasmall Ru nanoparticles on inorganic supports, with its amine and carboxyl groups serving as a surface-capping agent for the Ru nanoparticles and an anchor to inorganic supports, respectively. The catalytic activity of the size-controlled Ru nanoparticles with sub-2-nm size on various supports, such as TiO_2, CeO_2, and Vulcan carbon, revealed that a strong metal−support interaction of Ru nanoparticles, especially on carbon support, is responsible for a higher CH_4 selectivity during Fischer−Tropsch synthesis.

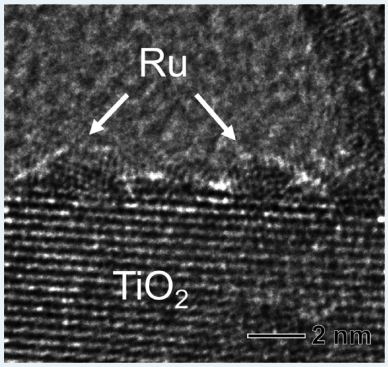

KEYWORDS: *ruthenium, nanoparticles, Fischer−Tropsch synthesis, product distribution, metal−support interaction*

1. INTRODUCTION

Noble metal nanoparticles are of particular interest because of their extensive uses in various catalysts.[1−10] The catalytic properties of the nanoparticles are highly sensitive to size, size distributions, and metal−support interactions. Generally, a reduction in size of metal nanoparticles provides a great opportunity to achieve a high surface-to-volume ratio and, thus, better efficiency in catalytic applications.[11] Great effort has been made to develop synthetic routes to obtain noble metal nanoparticles with sizes smaller than 5 nm, which typically involves the use of organic capping molecules or polymeric stabilizers.[12−17] Ruthenium (Ru) plays an important role in many catalytic reactions, including hydrogenation, CO oxidation, and the Fischer−Tropsch reaction.[18−22] Although Ru nanoparticles of variable size have been synthesized using different capping agents, there have been few reports on the synthesis of Ru nanoparticles in the sub-2-nm regime.[23,24]

We report here a simple aqueous-phase route to synthesize ultrasmall Ru nanoparticles with size <2 nm by introducing 6-aminohexanoic acid (AHA), a derivative of a natural amino acid, as a capping agent. The reported Ru nanoparticles exhibited an average size of 1.6−1.7 nm and a good homogeneous size distribution. We also found that both the amino and carboxyl groups of AHA play important roles in the formation of uniform, sub-2-nm Ru nanoparticles on the surface of the various inorganic supports, including TiO_2, CeO_2, and Vulcan carbon.

In the present study, by using the evenly distributed ultrasmall Ru nanoparticles on various supports, the roles of the Ru−support interaction for the product distribution during the Fischer−Tropsch synthesis (FTS) reaction were investigated. Even though the strengths of the metal−support interaction on many heterogeneous catalysts have been well-known to significantly alter the product distribution as a result of the changes in the electronic states of the supported metals, the intrinsic effects of the metal−support interaction have always been complicated because of their broad particle-size distributions while using conventional impregnation methods. The product distributions on cobalt-supported catalysts for FTS reaction are also known to be significantly affected by the particle size of the cobalt species, and CH_4 formation has been reported to be much higher on particles smaller than ∼6 nm, accompanied by lower intrinsic activity.[25−27]

In the present study, the homogeneously distributed sub-2-nm Ru nanoparticles were applied to elucidate the intrinsic metal−support interaction in regard to product distribution by characterizing the reducibility and the variation of the electronic states of Ru nanoparticles on TiO_2, CeO_2, and Vulcan carbon supports. Our approach provides a simple, environmentally benign, and readily scalable route to the synthesis of evenly distributed ultrasmall Ru nanoparticles supported on inorganic

Received: November 1, 2013
Revised: January 20, 2014
Published: February 21, 2014

   dx.doi.org/10.1021/cs401011q | ACS Catal. 2014, 4, 1054−1060

materials. By properly eliminating the effects of broad particle-size distribution, the strengths and oxidation states of Ru nanoparticles with the various supports are well correlated with the preferential CO hydrogenation activity to CH_4 because of their intrinsically different Ru−support interactions.

2. EXPERIMENTAL DETAILS

2.1. Synthesis of Ru Nanoparticles. In a typical synthesis, $RuCl_3$ (14 mg, supplied by Aldrich) and 6-aminohexanoic acid (AHA, 34 mg, Aldrich) were dissolved in 7 mL of aqueous dispersion containing 100 mg of anatase-phase TiO_2 powders (Aldrich) and then heated to 90 °C in air under magnetic stirring. Meanwhile, $NaBH_4$ (15 mg, Aldrich) was dissolved in 3 mL of deionized water at room temperature. The aqueous $NaBH_4$ solution was added to the reaction solution using a pipet. The reaction solution was maintained at 90 °C under magnetic stirring for 3 h and then cooled to room temperature. The sample, denoted as Ru/TiO_2, was collected by centrifugation and washed several times with water and acetone for further use in characterization and the FTS reaction. In the syntheses of Ru/CeO_2 and Ru/C nanostructures, 100 mg of CeO_2 powders (supplied by Aldrich) or Vulcan carbon powders (Vulcan XC-72R, supplied by BASF) were used instead of the TiO_2 powders, and the other experimental conditions were kept the same as in the synthesis of the Ru/TiO_2 nanostructures. The concentration of Ru on all supporting material was fixed at a weight percentage of 3.6 based on each support employed.

2.2. Catalytic Activity Measurements and Characterizations. The catalytic activities of FTS reaction of the as-prepared Ru nanoparticles on TiO_2, CeO_2, and Vulcan carbon support were investigated in a fixed-bed tubular reactor with an outer diameter of 9.5 mm. A 200 mg portion of the Ru nanoparticle-supported catalysts was loaded into the reactor and then reduced in situ under H_2 flow at 350 °C for 3 h. After reduction, the reactor was cooled to room temperature, and the reaction pressure was increased to 2.0 MPa. Syngas with a molar composition of $CO/H_2/N_2$ = 31.5/63.0/5.5 (with N_2 as an internal standard gas) was subsequently fed into the reactor. The reaction temperature was then increased to 230 °C at a fixed weight hourly space velocity of 4000 $L/kg_{cat}/h$ for a reaction duration of 40 h. The effluent gases from the reactor were analyzed by simultaneously using two detectors equipped in an online gas chromatograph (GC: YoungLin Acme 6100, South Korea) with a GS-GASPRO capillary column and a flame ionization detector, as well as a Carboxen 1000 packed column with a thermal conductivity detector (TCD) using Ar as a carrier gas. The reaction rate and product distribution were calculated through the carbon balance using the average values for a duration of 5 h after 35 h on stream at a steady state.

Transmission electron microscopy (TEM), high-resolution TEM (HRTEM), and high-angle annular dark-field scanning TEM (HAADF-STEM) images were captured using a JEOL 2100F microscope operated at 200 kV.

Temperature-programmed reduction (TPR) experiments were carried out to determine the reducibility of Ru nanoparticles on the various supports using a TPR apparatus (BELCAT-M, Bel Japan Inc., Japan). Prior to TPR experiments, the sample was pretreated in an He flow at 300 °C for 2 h to remove adsorbed water. A reducing gas of $5\%H_2$ balanced with He was passed over the sample at a flow rate of 30 mL/min with a heating rate of 10 °C/min from 50 to 1000 °C. The effluent gases were passed over a molecular sieve trap to remove the water formed during the TPR experiment, and they were analyzed by a GC equipped with TCD. The degree of reduction (%) of Ru nanoparticles on the supports was calculated from the consumed amount of H_2 below 350 °C divided by that below 650 °C.

Fourier transform infrared (FT-IR) spectroscopy was also performed to verify the adsorbed CO species on Ru nanoparticles on the supports using a Perkin-Elmer Spectrum 2000 instrument. Before measurement, a self-supported pellet sample in an FT-IR cell was reduced in situ at 350 °C for 3 h under H_2 flow, and it was subsequently purged with He for 1 h. CO gas with a flow rate of 30 cc/min was introduced to the self-supported sample at 50 °C for 30 min, and FT-IR spectra of the adsorbed CO species were collected at 100 °C after purging with He flow for 20 min. The characteristic peaks of adsorbed CO species at wave numbers around 2080 and 2170 cm^{-1} are assigned to peaks I and II, respectively, and the intensity ratio of peak II/peak I was also calculated using the integrated areas of each peak.

The electronic states of Ru nanoparticles on CeO_2 and Vulcan carbon support were characterized using X-ray photoelectron spectroscopy (XPS; Escalab MK-II). For the XPS analysis, an Al Kα monochromatized line (1486.6 eV) was adopted, and the vacuum level was kept around 10^{-7} Pa. The as-prepared and used FTS catalysts were previously pressed into thin pellets for analysis, and the binding energy (BE) was corrected using the reference BE of C 1s (284.6 eV).

3. RESULTS AND DISCUSSION

Evenly distributed Ru nanoparticles were synthesized in an aqueous solution by reducing $RuCl_3$ with $NaBH_4$ as a reducing agent in the presence of AHA as a capping agent by using metal oxide powders or carbon powders as supporting material to elucidate the intrinsic metal−support interaction for product distribution during the FTS reaction. Figure 1a,b shows typical TEM and HAADF-STEM images of Ru/TiO_2 nanostructures,

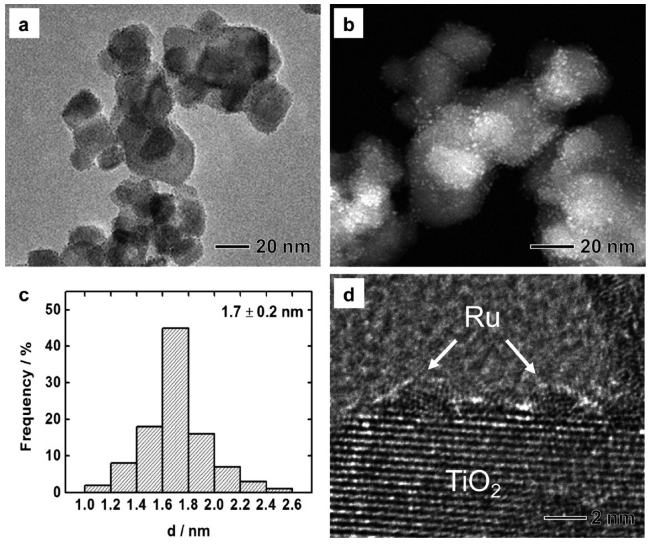

Figure 1. (a) TEM and (b) HAADF-STEM images of Ru/TiO_2 nanostructures synthesized by reducing $RuCl_3$ with $NaBH_4$ as a reducing agent in an aqueous solution containing AHA and TiO_2 powders. The reaction temperature was kept at 90 °C. (c) Particle size distribution of Ru nanoparticles supported on TiO_2 powders. (d) HRTEM image of Ru nanoparticles on the surface of TiO_2 powders.

dx.doi.org/10.1021/cs401011q | ACS Catal. 2014, 4, 1054−1060

respectively. These images clearly show that a number of small Ru nanoparticles were formed and evenly distributed on the entire surfaces of TiO_2 powders without a significant overlap between them. The formation of isolated Ru nanoparticles in the catalysts employed was not observed. The Ru nanoparticles on TiO_2 powders had an average size of 1.7 nm (Figure 1c). The Ru/TiO_2 nanostructures were further characterized by HRTEM. Figure 1d gives an HRTEM image of Ru nanoparticles on the surface of the TiO_2 powders, which reveals that the lattice fringes are not coherent across the interface between TiO_2 powders and Ru nanoparticles. This observation also indicates that Ru nanoparticles were grown nonepitaxially on the surface of TiO_2 powders.

Under the same preparation conditions as those in Figure 1a , except for the absence of AHA and TiO_2 powders for comparison, large Ru aggregates were obtained (Figure 2a). When the synthesis was conducted with the addition of AHA in the absence of TiO_2 powders, Ru nanoparticles of ~2 nm were obtained, although they assembled into a raspberry-like morphology (Figure 2b). When only TiO_2 support was added, the TiO_2 powders contained fewer Ru nanoparticles, and large Ru aggregates were observed separately from the TiO_2 support (Figure 2c). These results clearly show that AHA serves as an effective capping agent in the formation of small Ru nanoparticles and that our approach based on the use of both AHA and an inorganic support provides superb control over the formation and distribution of ultrasmall, sub-2-nm Ru nanoparticles on the inorganic supports.

For a better understanding of the role played in the synthesis of Ru/TiO_2 nanostructures by AHA, which has amino and carboxyl end groups, hexylamine or hexanoic acid was also used instead of AHA. When hexylamine was used as a capping agent, we observed the formation of sub-2-nm Ru nanoparticles separately from the TiO_2 powders (Figure 3a), indicating that the carboxyl group in AHA plays a key role in anchoring Ru nanoparticles to the TiO_2 surfaces. In the case of hexanoic acid, Ru nanoparticles were immobilized on the TiO_2 surfaces, but many of them aggregated with each other on the surface of the TiO_2 powders (Figure 3b). This result indicates that the amine group in AHA is responsible for the formation of Ru nanoparticles with a narrow size distribution. Therefore, we can suggest that the amine and carboxyl groups in AHA serve as a surface-capping agent for the Ru nanoparticles and the anchor to the support, respectively, as schematically shown in Figure 3c.

The AHA-stabilized Ru nanoparticles had a negatively charged surface, as determined by ζ potential measurement, with a ζ potential value of −21.5 mV at pH = 5.5, which could be attributed to the deprotonation of the carboxyl group in AHA and the formation of a carboxylate anion. Meanwhile, TiO_2 powders had a positively charged surface with a ζ potential value of +14.7 mV at pH = 5.5. The electrostatic attraction between the AHA-stabilized Ru nanoparticles and the positively charged surface of the TiO_2 powders may help the immobilization of the Ru nanoparticles on the TiO_2 support.

Our approach was also found to be readily applicable to the synthesis of sub-2-nm Ru nanoparticles immobilized on other inorganic and carbon supports, such as CeO_2 powders and Vulcan carbon powders. Figure 4 shows a representative TEM image and a particle size distribution of Ru nanostructures on CeO_2 powders prepared under the same conditions as those in Figure 1a, except that CeO_2 powders were added to the synthesis instead of TiO_2 powders. Ru nanoparticles with an average size of 1.6 nm were formed and uniformly distributed on the surface of the CeO_2 powders and can be designated as

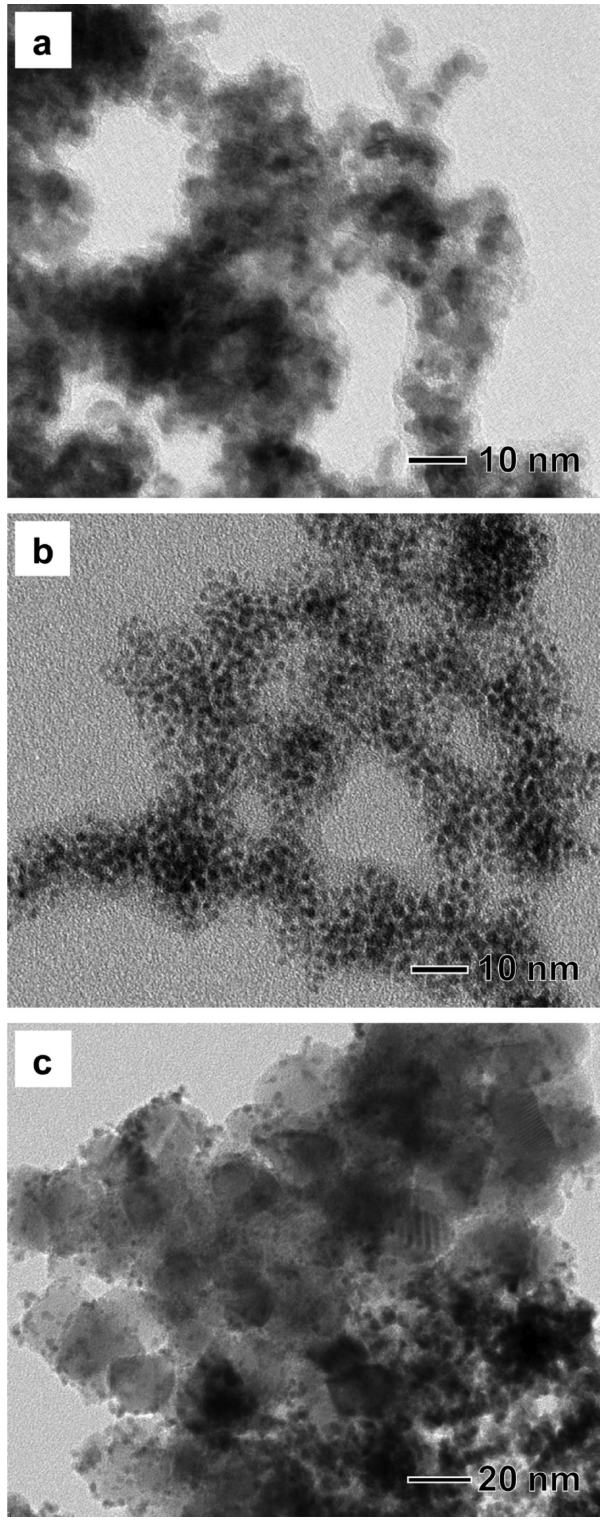

Figure 2. (a) TEM image of Ru nanoparticles prepared under the same conditions as those in Figure 1a, except that the synthesis was conducted in the absence of AHA and TiO_2 powders. (b) TEM image of Ru nanoparticles prepared under the same conditions as those in Figure 1a, except that the synthesis was conducted in the absence of TiO_2 powders. (c) TEM image of a Ru/TiO_2 catalyst prepared under the same conditions as those in Figure 1a, except that the synthesis was conducted in the absence of AHA.

dx.doi.org/10.1021/cs401011q | ACS Catal. 2014, 4, 1054−1060

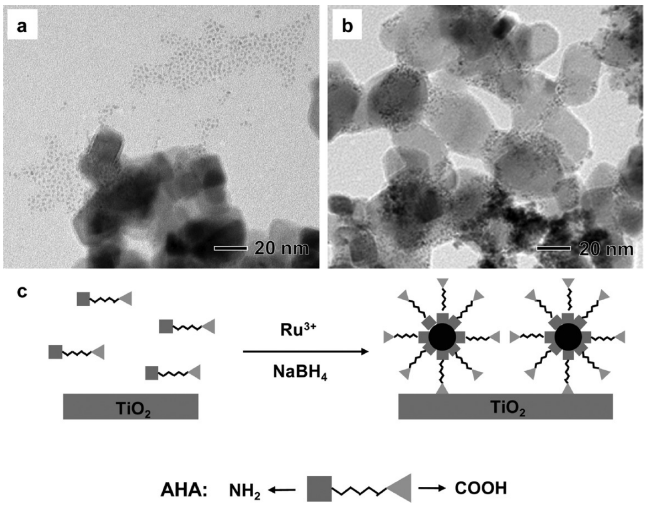

Figure 3. (a) TEM image of a Ru/TiO_2 catalyst prepared under the same conditions as those in Figure 1a, except that the synthesis was conducted in the presence of hexylamine instead of AHA. (b) TEM image of a Ru/TiO_2 catalyst prepared under the same conditions as those in Figure 1a, except that the synthesis was conducted in the presence of hexanoic acid instead of AHA. (c) A schematic illustration of AHA-stabilized Ru nanoparticles on the TiO_2 surface.

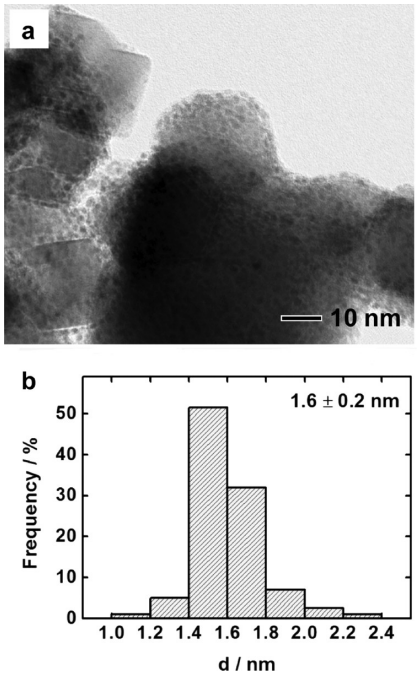

Figure 4. (a) TEM image of a Ru/CeO_2 catalyst prepared under the same conditions as those in Figure 1a, except that the synthesis was conducted in the presence of CeO_2 powders instead of TiO_2 powders. (b) Particle size distribution of Ru nanoparticles supported on CeO_2 powders.

dark field images. Vulcan carbon powders also possess positive charges on their surface, as indicated by the ζ potential measurement, +14.9 mV at pH 6. When Vulcan carbon powders were added to the synthesis instead of TiO_2 powders, we also observed the formation and uniform distribution of Ru nanoparticles with an average size of 1.6 nm on the entire surfaces of the carbon support (Figure 5) through the same synthetic mechanisms.

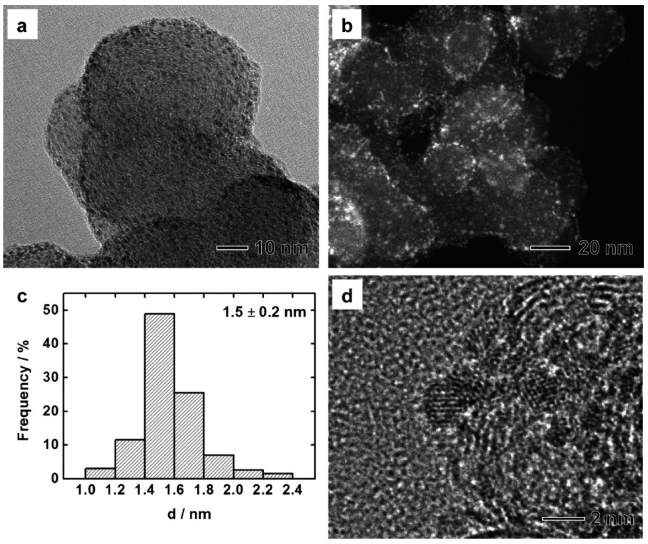

Figure 5. (a) TEM and (b) HAADF-STEM images of Ru/C nanostructures prepared under the same conditions as those in Figure 1a, except that the synthesis was conducted in the presence of Vulcan carbon powders instead of TiO_2 powders. (c) Particle size distribution of Ru nanoparticles supported on Vulcan carbon powders. (d) HRTEM image of Ru nanoparticles on the surface of Vulcan carbon powders.

The as-prepared nanostructured Ru catalysts were prereduced for the activity measurement, because the synthesized Ru nanoparticles were exposed to air during the drying step. The partially oxidized RuO_2 shell was formed by sacrificing the metallic Ru core, which was revealed by XPS analysis of Ru $3p_{3/2}$ peaks on the as-prepared catalysts, as shown in Supporting Information (SI) Figure S1. Interestingly, the partial oxidation of Ru nanoparticles with the main phase of RuO_2 species was observed to a significant extent on the Ru/C catalyst. In addition, the effects of chloride residues on the catalysts have been known to alter the catalytic activity significantly, but the amount of chloride residues in our presynthesis of Ru nanoparticles was not significant because of their preparation in a reduction atmosphere as well as in a reduction pretreatment under hydrogen flow. This was also confirmed by checking the chloride residues assigned to the BE around 199 eV from XPS analysis, and the residues were not always detected on the as-prepared catalysts, as shown in SI Figure S2.

The size-controlled Ru nanoparticles around 1.6 nm on TiO_2, CeO_2, and Vulcan carbon supports were investigated to elucidate the effects of metal−support interaction for the reducibility of Ru nanoparticles and the product distribution during FTS reaction. In general, the product distributions of FTS reaction on the supported metal catalysts for CO hydrogenation to hydrocarbons are known to be significantly affected by factors such as the particle size distribution of active metals as well as the morphologies, pore size of the supports, adsorption properties of the reactants and products, the amount of carbon deposition, the extent of aggregation of metal particles, and the electronic properties, which can be through the different interactions with supports by a structure-sensitive reaction mechanism.[25−27] However, these distinctive effects have not been clearly investigated because the mixed characteristics of these complicated contributions can alter the catalytic activity and product distribution simultaneously.

dx.doi.org/10.1021/cs401011q | ACS Catal. 2014, 4, 1054−1060

In the case of cobalt-based FTS catalysts, the small Co_3O_4 particles with size below 6 nm, which have a large portion of lower-coordinated surface sites, are responsible for a lower intrinsic activity and a higher CH_4 selectivity. This can be attributed to the strong adsorption character of CO molecules by blocking edge/corner sites through molecular adsorption of the CO molecules instead of H_2-assisted dissociative adsorption of CO molecules on larger cobalt particles with size above 10 nm.[25,28−30] On a Ru-based catalyst, the FTS reaction has been reported to occur through CO dissociation on the stepped sites, which is responsible for the carbon-rich environment by accumulating CH_x species through forming long-chain hydrocarbons.[31] However, because the unique metal−support interaction for the FTS reaction to the product distribution using the supported size-controlled metal particles on the various supports has scarcely been reported until now, the size-controlled Ru nanoparticles with size around 1.6 nm on the various supports were investigated in the present study to elucidate the intrinsic effects of metal−support interaction on the product distribution for the FTS reaction.

The reduction patterns of partially oxidized Ru nanoparticles on the various supports are displayed in Figure 6. The single characteristic reduction peak of Ru oxides[32] was observed below 400 °C, and the maximum reduction peaks were found to be around 256, 252, and 330 °C on Ru/TiO_2, Ru/CeO_2, and Ru/C, respectively. The peak at a lower reduction temperature can be attributed to the easy reduction of surface Ru oxides to metallic particles, especially on Ru/TiO_2. The observed higher reduction temperature peak at 792 °C on Ru/CeO_2 can be attributed to the partial reduction of CeO_2 crystallites. The degree of reduction (defined as the amount of H_2 consumed below 350 °C divided by that below 650 °C) is also summarized in Table 1. The values were found to be 88.7, 90.7, and 66.4% on Ru/TiO_2, Ru/CeO_2, and Ru/C, respectively. The higher degree of reduction is well-known to be responsible for the formation of higher-molecular-weight hydrocarbons because of the facile dissociative adsorption of CO molecules on the reduced metal surfaces.[31] Therefore, the Ru/CeO_2 catalyst, which showed a lower maximum reduction temperature and a higher degree of reduction, seems to be the proper catalyst to form higher-molecular-weight hydrocarbons.

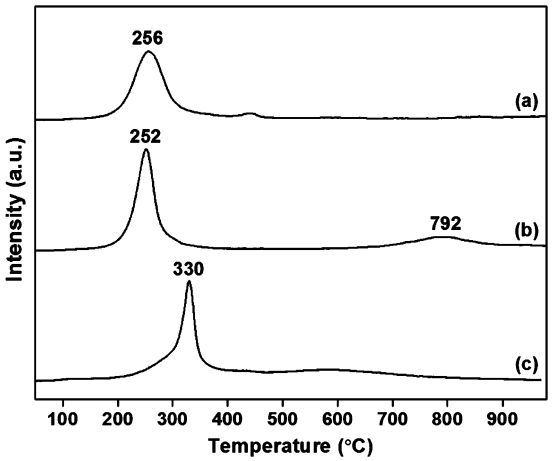

Figure 6. TPR profiles of sub-2-nm Ru nanoparticles on the various supports for (a) Ru/TiO_2, (b) Ru/CeO_2, and (c) Ru/C.

The reduction states of Ru nanoparticles on the various supports were further characterized by analyzing the types of adsorbed CO molecules through FT-IR experiments, as shown in Figure 7. The characteristic adsorption peaks of CO

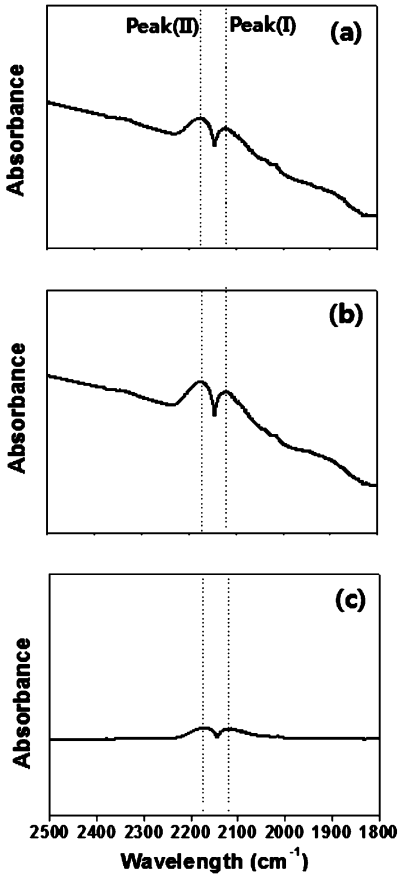

Figure 7. FT-IR spectra of adsorbed CO molecules. The distinctive absorbance peaks of adsorbed CO molecules at 2080 and 2170 cm^{-1} are assigned to peaks I and II, respectively, for (a) Ru/TiO_2, (b) Ru/CeO_2, and (c) Ru/C.

Table 1. Catalytic Activity and Summarized Results of Characterizations of the Ru Nanoparticles Supported on Various Supports

		product distribution (C mol %)				TPR	FT-IR of adsorbed CO
catalysts	reaction rate ($\mu mol \cdot g^{-1} \cdot s^{-1}$)	C_1	C_2-C_4	C_5^+	$O/(O+P)^a$	reduction degree (%)	ratio peak II/peak I
Ru/TiO_2	0.66	9.8	18.0	72.2	0.65	88.7	0.263
Ru/CeO_2	0.60	4.7	18.6	76.7	0.76	90.7	0.195
Ru/C	0.77	21.7	15.1	63.2	0.44	66.4	0.302

[a]The olefin selectivity based on C mol % in the range of C_2-C_4 hydrocarbons is defined as the amount of olefins divided by total hydrocarbons (olefin (O) + paraffin (P)).

dx.doi.org/10.1021/cs401011q | ACS Catal. 2014, 4, 1054−1060

molecules at wave numbers around 2080 and 2170 cm^{-1} were observed on all catalysts employed. These absorbance peaks can be assigned to the polycarbonyl species adsorbed on the partially reduced Ru oxide surfaces. The band at 2080 cm^{-1} can be attributed to linearly bonded CO molecules on the reduced Ru metals, and the bands at 2170 cm^{-1} can be assigned to the strong adsorption of CO molecules on the partially reduced Ru metal surfaces, which have a higher oxidation state by acting as a simple σ donor.[32,33] The characteristic absorption peaks of CO molecules are assigned to peak I and peak II for wavenumbers 2080 and 2170 cm^{-1}, respectively. The intensity ratios of peak II/peak I are summarized in Table 1. The ratios were found to be 0.263, 0.195, and 0.302 for the as-prepared Ru/TiO_2, Ru/CeO_2, and Ru/C, respectively. The higher value observed on Ru/C suggests the dominant presence of less reduced Ru nanoparticles, and the values correspond well to the degree of reduction, as shown in the TPR experiments.

To further clarify the extent of Ru aggregation after the FTS reaction, TEM analyses were carried out on the used FTS catalysts, as shown in Figure 8. The variations of morphologies and particle sizes of the Ru nanoparticles were kept insignificant by maintaining the evenly distributed particles around 2−3 nm in size, even after 40 h of reaction on all the tested catalysts. This observation also supports that the different product distributions can be attributed mainly to the unique metal−support interactions by eliminating the effects of broad Ru particle size distribution. In the case of cobalt-based FTS catalysts, the small size of cobalt particles below 6 nm can increase the CH_4 selectivity as a result of the strong metal−support interaction or facile oxidation of reduced metallic cobalt by the water formed.[25] Therefore, the present catalytic system seems to demonstrate a unique metal−support interaction for the product distribution of the FTS reaction.

The catalytic activities and product distributions are summarized in Table 1. The reaction rates (micromoles of consumed $CO/g_{cat}/s$) were found to be in the range of 0.60−0.77, with small variation. However, the product distributions were largely altered according to the type of supports. The higher selectivity to CH_4 around 21.7% was observed on Ru/C, which showed the lowest degree of reduction and a higher oxidation state confirmed by TPR and FT-IR analyses of adsorbed CO molecules. The amount of CH_4 formation was found to be in the order of Ru/CeO_2 < Ru/TiO_2 < Ru/C, and this trend was well correlated with the results of TPR and FT-IR analyses. A lower degree of reduction and higher oxidation state of the evenly distributed size-controlled Ru nanoparticles are attributed mainly to a stronger metal−support interaction, and its strength with support also significantly alters the product distribution by varying the adsorption strength of CO molecules on active metallic Ru nanoparticles.

The oxidation states of Ru nanoparticles on Ru/TiO_2, Ru/CeO_2, and Ru/C were further confirmed by XPS analysis using the used FTS catalysts, as shown in SI Figure S3. Increased Ru $3d_{5/2}$ peak intensities of metallic Ru particles were observed on all FTS catalysts used, and the partial oxidation of the RuO_2 shell was maintained even after FTS reaction by showing the same trend as the as-prepared catalysts (SI Figure S1). It can also be responsible for showing a different product distribution of the FTS reaction.

To verify the effects of the oxidation states of Ru nanoparticles on the product distribution, the catalytic activities on Ru/supports were also further measured at a different reduction temperature of 100 °C for 3 h; the results are summarized in SI Table S1. The size-controlled Ru−support catalysts, which were reduced at a lower temperature, showed a suppressed catalytic activity with a higher CH_4 selectivity compared with catalysts reduced at 350 °C. It can be suggested that a strong metal−support interaction can induce a higher oxidation state of Ru nanoparticles, especially on Ru/C, and it simultaneously increased CH_4 selectivity on the size-controlled Ru-based catalysts. The somewhat higher reaction rate on Ru/C, which showed the highest CH_4 selectivity, can also be attributed to the fast formation rate of CH_4 by CO hydrogenation compared with that of the higher-molecular-weight linear hydrocarbons.[34,35] The lower olefin selectivity of

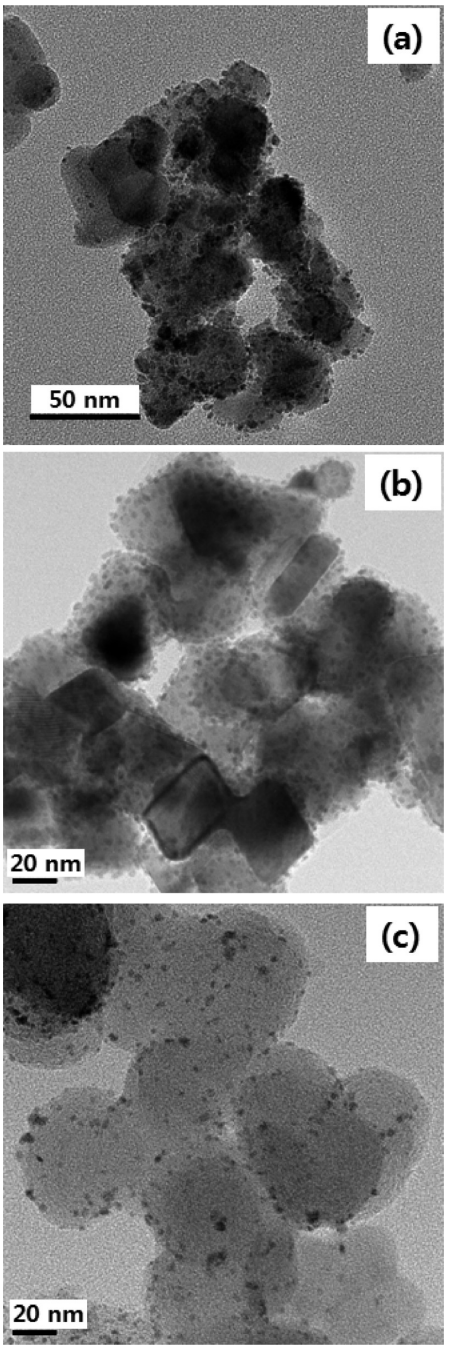

Figure 8. TEM images of Ru nanoparticles on (a) Ru/TiO_2, (b) Ru/CeO_2, and (c) Ru/C catalyst after FTS reaction. The aggregation of sub-2-nm Ru nanoparticles was not significant, even after 40 h duration of FTS reaction.

dx.doi.org/10.1021/cs401011q | ACS Catal. 2014, 4, 1054−1060

0.44 (O/(O + P) value) observed on Ru/C seems to be due to the fast hydrogenation rate on the partially reduced Ru oxide surfaces.

In summary, the strengths of the metal−support interaction on various supports with the size-controlled Ru nanoparticles around 1.6 nm on the as-prepared catalysts were well correlated with the product distribution of hydrocarbons for FTS reaction. The stronger interaction of Ru nanoparticles with the support is responsible for a higher CH_4 selectivity as a result of the electron-poor character of the partially reduced Ru oxides, and it was fundamentally verified by eliminating the complicated effects of broad particle size distribution and just by comparing the intrinsic character of the metal−support interactions.

4. CONCLUSIONS

A simple aqueous-phase synthesis of Ru nanoparticles with sizes in the sub-2-nm regime by introducing AHA as a capping agent was well demonstrated. It showed that AHA plays an important role in the formation and uniform deposition of ultrasmall Ru nanoparticles with an even size distribution on the surface of various inorganic supports, including TiO_2, CeO_2, and Vulcan carbon powders. For CO hydrogenation to hydrocarbons, the catalytic activities on the evenly size-controlled Ru nanoparticles on the various supports reveal that the partially reduced Ru particles with sub-2-nm size are responsible for a higher CH_4 selectivity as a result of the strong metal−support interaction. The nanostructures consisting of AHA-stabilized Ru nanoparticles supported on inorganic powders may find use in many catalytic applications, and we expect that our methodology can be applied to the synthesis of ultrasmall nanoparticles made of other noble metals for various catalytic applications.

■ ASSOCIATED CONTENT

Supporting Information

The results of XPS analysis on the as-prepared and the used FTS catalysts are included in Figures S1, S2, and S3. Catalytic activities on Ru/supports at different reduction temperatures of 100 and 350 °C are also summarized in Table S1. This information is available free of charge via the Internet at http://pubs.acs.org.

■ AUTHOR INFORMATION

Corresponding Authors

*E-mail: blim@skku.edu.

*E-mail: finejw@skku.edu.

Author Contributions

T. Koh and H. M. Koo contributed equally.

Notes

The authors declare no competing financial interest.

■ ACKNOWLEDGMENTS

This work was supported by the Basic Science Research Program (No. 2012R1A2A2A02013876, No. 2011-0009852, and No. 2011-0009003) through the National Research Foundation (NRF) of Korea funded by the Ministry of Education, Science, and Technology (MEST).

■ REFERENCES

(1) Ahmadi, T. S.; Wang, Z. L.; Green, T. C.; Henglein, A.; El-Sayed, M. A. *Science* **1996**, *272*, 1924−1926.

(2) Narayanan, R.; El-Sayed, M. A. *J. Phys. Chem. B* **2003**, *107*, 12416−12424.

(3) Jana, N. R.; Peng, X. G. *J. Am. Chem. Soc.* **2003**, *125*, 14280−14281.

(4) Song, Y. J.; Yang, Y.; Medforth, C. J.; Pereira, E.; Singh, A. K.; Xu, H. F.; Jiang, Y. B.; Brinker, C. J.; van Swol, F.; Shelnutt, J. A. *J. Am. Chem. Soc.* **2004**, *126*, 635−645.

(5) Teng, X. W.; Yang, H. *Nano Lett.* **2005**, *5*, 885−891.

(6) Tian, N.; Zhou, Z. Y.; Sun, S. G.; Ding, Y.; Wang, Z. L. *Science* **2007**, *316*, 732−735.

(7) Wang, X.; Li, Y. D. *Chem. Commun.* **2007**, *28*, 2901−2910.

(8) Wang, C.; Daimon, H.; Lee, Y.; Kim, J.; Sun, S. *J. Am. Chem. Soc.* **2007**, *129*, 6974−6975.

(9) Wang, L.; Yamauchi, Y. *J. Am. Chem. Soc.* **2009**, *131*, 9152−9153.

(10) Tsung, C. K.; Kuhn, J. N.; Huang, W. Y.; Aliaga, C.; Hung, L. I.; Somorjai, G. A.; Yang, P. *J. Am. Chem. Soc.* **2009**, *131*, 5816−5822.

(11) Plomp, A. J.; Vuori, H.; Krause, A. O.; Jong, K. P.; Britter, J. H. *Appl. Catal., A* **2008**, *351*, 9−15.

(12) Ahmadi, T. S.; Wang, Z. L.; Henglein, A.; El-Sayed, M. A. *Chem. Mater.* **1996**, *8*, 1161−1163.

(13) Petroski, J. M.; Wang, A. L.; Green, T. C.; El-Sayed, M. A. *J. Phys. Chem. B* **1998**, *102*, 3316−3320.

(14) Yamamoto, K.; Imaoka, T.; Chun, W.-J.; Enoki, O.; Katoh, H.; Takenaga, M.; Sonoi, A. *Nat. Chem.* **2009**, *1*, 397−402.

(15) Li, Y.; Huang, Y. *Adv. Mater.* **2010**, *22*, 1921−1925.

(16) San, B. H.; Kim, S.; Moh, S. H.; Lee, H.; Jung, D.-Y.; Kim, K. K. *Angew. Chem., Int. Ed.* **2011**, *50*, 11924−11929.

(17) Tanaka, S.-I.; Miyazaki, J.; Tiwari, D. K.; Jin, T.; Inouye, Y. *Angew. Chem., Int. Ed.* **2011**, *50*, 431−435.

(18) Liu, F.; Lee, J. Y.; Zhou, W. J. *Adv. Funct. Mater.* **2005**, *15*, 1459−1464.

(19) Nowicki, A.; Zhang, Y.; Leger, B.; Rolland, J. P.; Bricout, H.; Monflier, E.; Roucoux, A. *Chem. Commun.* **2006**, 296−298.

(20) Ning, J. B.; Xu, J.; Liu, J.; Lu, F. *Catal. Lett.* **2006**, *109*, 175−183.

(21) Joo, S. H.; Park, J. Y.; Renzas, J. R.; Butcher, D. R.; Huang, W.; Somorjai, G. A. *Nano Lett.* **2010**, *10*, 2709−2713.

(22) Nurunnabi, M.; Murata, K.; Okabe, K.; Inaba, M.; Takahara, I. *Catal. Commun.* **2007**, *8*, 1531−1537.

(23) Pan, C.; Pelzer, K.; Rhilippot, K.; Chaudret, B.; Dassenoy, F.; Lecante, P.; Casanove, M.-J. *J. Am. Chem. Soc.* **2001**, *123*, 7584−7593.

(24) Chen, Y.; Yong, K.; Li, J. *Mater. Lett.* **2008**, *62*, 1018−1021.

(25) Khodakov, A. Y.; Chu, W.; Fongarland, P. *Chem. Rev.* **2007**, *107* (5), 1692−1744.

(26) Cheng, K.; Kang, J.; Huang, S.; You, Z.; Zhang, Q.; Ding, J.; Hua, W.; Lou, Y.; Deng, W.; Wang, Y. *ACS Catal.* **2012**, *2*, 441−449.

(27) Bae, J. W.; Park, S. J.; Woo, M. H.; Cheon, J. Y.; Ha, K. S.; Jun, K. W.; Lee, D. H.; Jung, H. M. *ChemCatChem* **2011**, *3*, 1342−1347.

(28) den Breejen, J. P.; Radstake, P. B.; Bezemer, G. L.; Bitter, J. H.; Froseth, V.; Holmen, A.; de Jong, K. P. *J. Am. Chem. Soc.* **2009**, *131*, 7197−7203.

(29) Borg, O.; Dietzel, P. D. C.; Spjelkavik, A. I.; Tveten, E. Z.; Walmsley, J. C.; Diplas, S.; Eri, S.; Holmen, A.; Rytter, E. *J. Catal.* **2008**, *259*, 161−164.

(30) Tuxen, A.; Carenco, S.; Chintapalli, M.; Chuang, C. H.; Escudero, C.; Pach, E.; Jiang, P.; Borondics, F.; Beberwyck, B.; Alivisatos, A. P.; Thornton, G.; Pong, W. F.; Guo, J.; Perez, R.; Besenbacher, F.; Salmeron, M. *J. Am. Chem. Soc.* **2013**, *135*, 2273−2278.

(31) Chen, J.; Liu, Z. P. *J. Am. Chem. Soc.* **2008**, *130*, 7929−7937.

(32) Carballo, J. M. G.; Finocchio, E.; Garcia-Rodriguez, S.; Ojeda, M.; Fierro, J. L. G.; Busca, G.; Rojas, S. *Catal. Today* **2013**, *214*, 2−11.

(33) Kumar, N.; Jothimurugesan, K.; Stanley, G. G.; Schwartz, V.; Spivey, J. J. *J. Phys. Chem. C* **2011**, *115*, 990−998.

(34) Kwack, S. H.; Park, M. J.; Bae, J. W.; Park, S. J.; Ha, K. S.; Jun, K. W. *Fuel Process. Technol.* **2011**, *92*, 2264−2271.

(35) van Santen, R. A.; Markvoort, A. J.; Ghouri, M. M.; Hilbers, P. A. J.; Hensen, E. J. M. *J. Phys. Chem. C* **2013**, *117*, 4488−4504.